

Validation of a Dynamic Inflow Model Based on a Flight Dynamics Model and a Lattice-Boltzmann Fluid Solver Using Flight Test Data

Jakob Bludau *

Jürgen Rauleder †

Manfred Hajek ‡

*Institute of Helicopter Technology
Technical University of Munich, 80333 Munich, Germany*

A fully-coupled, real-time-capable fluid dynamics/flight dynamics simulation was developed, that is validated against flight test data measured with a MBB Bo-105 helicopter. The highly-efficient Lattice-Boltzmann based fluid dynamics solver and the blade element based flight dynamics code were coupled through the rotor thrust and inflow. This dynamic inflow model extracted the inflow velocities from the computed flow field and passed them to the flight dynamics code to predict thrust and rotorcraft motion. The local rotor thrust was imposed on the fluid cells comprising the rotor disk. The advantage of this two-way coupled approach is that it enables the real-time calculation of the flow environment and the dynamic inflow into the rotors without prior knowledge of the flow field, and it allows to model the influence of arbitrary moving objects in the vicinity of the rotorcraft on the fluid mechanics and flight dynamics at simulation run-time. Power requirements and controls in trimmed stationary forward flight were predicted well by the new model. The on-axis response of the helicopter to pilot step inputs also correlated well with the flight test data. The off-axis response showed the correct trends, but the amplitudes were mostly underpredicted. This underprediction was similar to results obtained using the Pitt-Peters inflow model instead of the new modeling approach. The results gave confidence in the developed computational model, although areas for improvement were also identified. In the longer term, this new modeling approach may enable more realistic pilot training for challenging operations such as ship deck landings, where rapid changes to the flow field and the environment around the rotorcraft affect its flight dynamics.

Nomenclature

cg	Coordinate system in the center of gravity
d	Fluid cell length in flow solver, m
Δ	Difference from trimmed state
I_{ij}	Entry ij of inertia tensor, kgm^2
κ	Induced power factor
l_{bm}	Coordinate system of the fluid solver
N	Rotational velocity of the main rotor, rad/s
N_0	Reference rotational velocity of main rotor, rad/s
$N_{l_{bm}}$	Cells per edge of cubic domain in the fluid solver
N_Ψ	Number of points in circumferential direction
N_R	Number of blade elements
P_{mr}	Power required by the main rotor, kW
Φ	Roll attitude of the helicopter, deg
Ψ	Heading of the helicopter, deg

p_{cg}	Angular velocity in rolling (x_{cg} -axis), deg/s
q_{cg}	Angular velocity in pitching (y_{cg} -axis), deg/s
R	Main rotor radius, m
r_{cg}	Angular velocity in yawing (z_{cg} -axis), deg/s
ρ	Local air density, kg/m^3
ρ_0	Reference air density at mean sea level, kg/m^3
Θ	Pitch attitude of the helicopter, deg
u_{cg}	Velocity in x_{cg} -axis, m/s
v_0^i	Mean induced velocity component, m/s
v_c^i	Cosine component of induced velocity, m/s
v_s^i	Sine component of induced velocity, m/s

Introduction

To train pilots in simulators for complicated flight situations such as the flight in the wake of large objects (e.g., ship airwakes) or in time-varying ground effect, the flight dynamics model has to be able to adequately represent the resulting changes in dynamic reaction and handling of the rotorcraft when flying in such conditions. As the rotorcraft motion is mainly defined by the forces and moments produced by and acting on the rotors, the effects of the ground

* Graduate Research Assistant, jakob.bludau@tum.de

† Lecturer, juergen.rauleder@tum.de

‡ Professor and Department Head, hajek@tum.de

Presented at the 43rd European Rotorcraft Forum, Milano, Italy, September 12–15, 2017. Copyright ©2017 by the authors except where noted. All rights reserved. Published by CEAS with permission.

(or other solid structures) and the changing flow field on the rotors are of particular importance. These interactional effects with the surroundings (i.e., wake–structure interaction and rapidly changing flow gradients) manifest in a distortion of the rotor wake and in a change in inflow into the rotors, hence affecting the flight dynamics of the rotorcraft.

To partially capture this behavior, established models such as the Pitt-Peters dynamic inflow model [1] have been modified and extended to provide more flexibility and generality, e.g. [2–4]. A comprehensive overview of the development and evolution of inflow models is given by Peters [5]. Despite their efficiency and success, these inflow models are not able to represent the influence of arbitrary objects surrounding the helicopter on its flight dynamics. RANS-based methods provide this capability but cannot be computed in real-time [6–8]. Therefore, to provide a real-time capable inflow model to be used in flight simulators, in this case, computations of RANS-based fluid solvers have to be tabulated beforehand, i.e., prior knowledge of the flow field is required. Another approach uses computationally more efficient free vortex wake methods on graphics cards, that can achieve real-time capability while also offering high flexibility to tailor models towards the needed fidelity [9]. However, these methods are not well suited for situations where complex (moving or non-moving) geometries, such as in urban environments or on ship decks, interact with the external flow (e.g., winds) and the rotor wake.

Another modeling approach to calculate the rotor inflow and the rotor wake including the effects of the surroundings was presented in previous work by the authors [10]. The presented dynamic inflow model was shown to be able to capture the distortion of the rotor wake due to the wake of moving and non-moving objects near the rotorcraft without any prior knowledge except for the geometry of these objects. Because of its real-time capability, this fully-coupled fluid dynamics/flight dynamics model can be used in piloted flight simulations.

Although partial validation was done [10] for this computational model, a more extensive validation is still necessary. In Ref. [10] the main rotor power, pilot inputs and the resulting dynamic reaction of the inflow were compared to the results obtained by the Pitt-Peters model [1]. Nevertheless, to prove the capabilities and fidelity of the new model, and its practicality to be used in piloted flight simulations, the system response of the rotorcraft when subjected to pilot inputs has to agree with the measured response in actual flight. Therefore, the validation of the developed inflow model was extended by comparisons to flight test data.

The flight tests, that were conducted and provided by the German Aerospace Center (DLR) using an MBB Bo-105 C helicopter, were used to evaluate the fidelity of the model and the practicality to be used in flight simulators. Thus, the focus of the current work is on the reaction of the helicopter to the pilot control inputs. Power and control requirements in trimmed stationary forward flight, and the

dynamic response of the rotorcraft to pilot inputs were analyzed and correlated to the flight test data. Because of its extensive use in rotorcraft flight simulations, the dynamic inflow model of Pitt and Peters [1] in the implementation following Peters and Haquang [11] was also included in the comparisons.

Modeling Approach

The flight dynamics model described in more detail in Ref. [10] consisted of a blade element based rotor dynamics code that was coupled with a Lattice-Boltzmann based fluid dynamics solver to calculate the forces of the main rotor. A mechanical six-degree-of-freedom model for the fuselage together with measured lift and drag polars to calculate aerodynamic forces on fuselage and empennage were used. For the blade element based rotor dynamics code, the main rotor was modeled using fully articulated, rigid blades allowing lead-lag, flap, and feathering motion. Each blade was discretized with $N_R = 8$ blade elements in radial direction. In circumferential direction, the rotor was discretized with $N_\Psi = 72$ evenly spaced azimuthal positions, i.e., every five degrees of rotor azimuth.

The aerodynamic forces that acted on the blade at every one of these positions were calculated using measured profile polars for lift and drag of the NACA 23012 airfoil. The resulting aerodynamic forces were passed to the Lattice-Boltzmann solver that calculated the entire flow field around the rotorcraft including the flow through the rotor, and then handed the result back to the blade element code. With this, the dynamic inflow and the rotor forces were calculated using the blade element code coupled with the fluid dynamics solver.

The fluid solver used a cubic computational domain with an edge length of $4R$, with R being the main rotor radius; see Fig. 1. The cubic grid was fixed to the rotorcraft and an arbitrary Lagrangian-Eulerian moving grid approach [12] was used to reduce computational expense by minimizing the physical size of the computational domain. The rotor hub was located one R from the top of the domain and centered in the other two directions. This ensured that $3R$ were left below the rotor to be able to fully capture the ground effect that becomes insignificant at heights greater than $3R$ above the ground plane [13]. The resolution N_{lbm} of the simulation was defined as the number of cells per edge length of the cubic domain, which resulted in a fluid cell length of $d = \frac{4R}{N_{\text{lbm}}}$.

Only the linear/harmonic coupling mode as discussed in Ref. [10] was used. In this mode, the coefficients of the harmonic analysis of the thrust of all blades were sent to the fluid dynamics solver to calculate the flow field. The coefficients of a linearization of the velocity, as used in the Pitt-Peters model, were sent back to the flight dynamics code to calculate the forces and moments of the rotor. This way the model was fully coupled and comparable to the Pitt-Peters model.

To represent objects inside the fluid solver’s computational domain, the position and shape of (moving and non-moving) objects and terrain were extracted from a database and modeled using bounce-back wall boundary conditions [14]. The fuselage of the helicopter was also modeled using the same wall boundary conditions. By updating the position and size of the objects, the fluid solver was able to capture changing terrain and obstacles during run-time using ray-tracing algorithms. With this the effect of these solid objects on the flow field, i.e., information about the flow modifications, was transported to the rotors by the fluid solver. The resulting perturbation of the inflow changes the thrust and moments that the rotor produces, thereby changing the flight dynamics and handling qualities of the helicopter. Therefore, the pilot is able to feel the influence that the surroundings have on the helicopter.

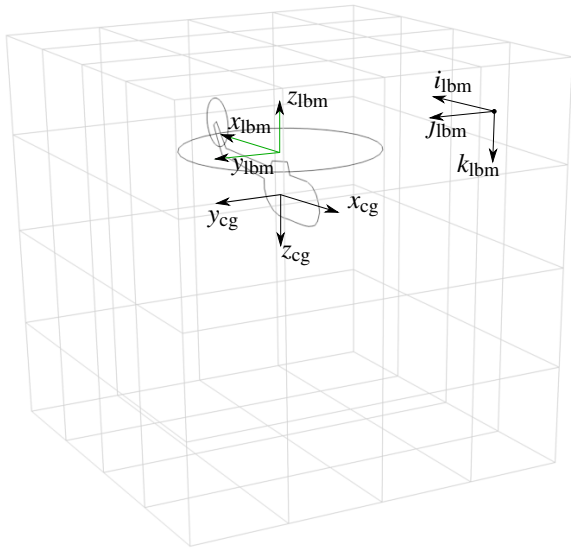


Fig. 1: Fluid domain with an exemplary grid of $N_{lbm} = 4$, coordinate system in the center of gravity, cg, and coordinate system and grid indices of the Lattice-Boltzmann solver, lbm. For simplicity, cell edges inside the domain are not shown. From Ref. [10].

The inflow into the tail rotor was not modeled using the coupled approach because this would result in extremely poor spatial resolutions. Instead, its inflow was calculated using the dynamic inflow model of Pitt and Peters [1]. This also allowed for a better comparison of the effects of the inflow models on the main rotor alone. Both rotors were modeled as steady-state rotors in the flight dynamics code and as actuator disks in the fluid solver following the discussion in Ref. [10]. Using the steady-state assumption in transient maneuvers, the rotor reacts instantaneously to changes in the inflow or the controls. Nevertheless, for low-frequency control inputs or low-frequency variations of the inflow into the rotors, this assumption was found valid because the blade motion adjusted after about one rotor revolution, which is very fast compared to the reaction of the

rotorcraft [15]. Because the current paper focuses on the validation of the model and not the model development itself, a more detailed discussion on the modeling approach is given in Ref. [10].

Results and Discussion

The flight test data used for model validation were obtained by DLR Braunschweig in the IBIS project. The used helicopter was a MBB Bo-105 C with a take-off weight of 2200 kg, rectangular blades with a linear twist of -6.2 deg in the profiled section (NACA 23012), and a main rotor radius of $R = 4.92$ m. The rotorcraft center of gravity was located 0.03 m forward and 1.48 m below the center of the main rotor hub. The mass distribution yielded the following moments of inertia in the cg-system (as shown in Fig. 1): $I_{xx} = 1433 \text{ kgm}^2$, $I_{yy} = 4973 \text{ kgm}^2$, $I_{zz} = 4099 \text{ kgm}^2$, and $I_{xz} = 660 \text{ kgm}^2$. For all comparisons in this paper, the same rotorcraft was simulated using the fully-coupled inflow model [10] and the Pitt-Peters inflow model [1].

Trimmed Stationary Forward Flight

The first comparison concerns the power consumption of the main rotor, the attitudes of the helicopter, and the control inputs for trimmed forward flight at various flight speeds. The required main rotor power, P_{mr} , is shown in Fig. 2. It was normalized by the density ratio to compare to the flight test data at various heights and environmental conditions [16].

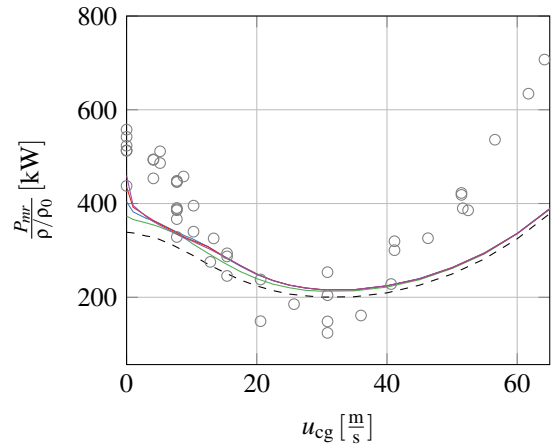


Fig. 2: Total power required by main rotor over forward flight velocity, u_{cg} . Results obtained by the fully-coupled dynamic inflow model for $N_{lbm} = 32$ (—), 64 (—), 128 (—), and 192 (—). Pitt-Peters model (---) and flight test measurements (○) for comparison.

For low forward speeds of up to $10 \frac{\text{m}}{\text{s}}$ the power predicted by the fully-coupled model and the Pitt-Peters model was lower than the power consumption measured in the flight tests. In the region of $u_{cg} = 10 - 40 \frac{\text{m}}{\text{s}}$ the power calculated using either of the inflow models agreed well

with the flight test data. For velocities beyond $u_{cg} = 40 \frac{m}{s}$ the flight tests showed greater power consumption compared to the models, and a diverging trend with further increasing forward flight speed. Furthermore, the computed hover power required by the fully-coupled model did not converge with increasing resolution of the fluid dynamics solver, which was already investigated and discussed in Ref. [10].

As both inflow models were based on the momentum theory (without any corrections), they underpredicted the induced power because they did not account for non-ideal effects [13, 15]. In contrast, Fig. 3 shows the main rotor power predicted by both inflow models using an induced power factor of $\kappa = 1.25$. The high value for κ is a reasonable assumption because of the relatively old rotor design of the MBB Bo-105 C using rectangular, weakly linearly twisted blades with a twist rate of $-6.2 \text{ deg}/r$, with r being the length of the profiled blade.

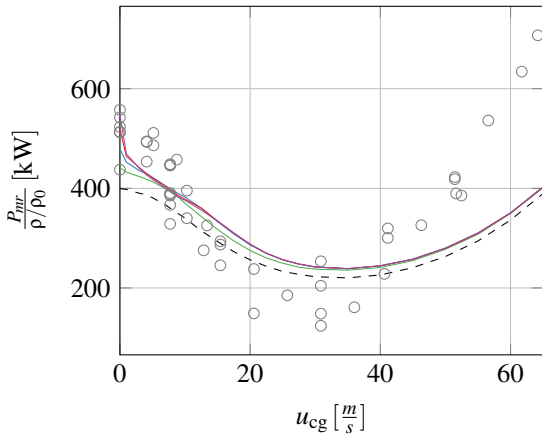


Fig. 3: Total power required by main rotor using $\kappa = 1.25$ for the induced power, plotted over forward flight velocity, u_{cg} . Results obtained by the fully-coupled dynamic inflow model for $N_{lbm} = 32$ (—), 64 (—), 128 (—), and 192 (—). Pitt-Peters model (---) and flight test measurements (○) for comparison.

Using the discussed correction for the induced power, the total power predicted by both inflow models correlated well with the flight test data for forward speeds of up to $u_{cg} = 40 \frac{m}{s}$. For higher forward speeds, the required power was still underpredicted compared to the flight test data. This underprediction was caused partly by the induced power that increases again at high forward flight velocities because of the low loading on the edges of the rotor disk [17], an effect that was not modeled. The second and dominant contribution to the difference in power was attributed to the measured drag polar for the fuselage, because it did not incorporate the effects of flow separation and increased pressure drag at higher speeds. This reasoning was also supported by the good agreement in the pitch attitude, Θ , of the fuselage (shown in Fig. 4), a result by which (a potentially incorrect) pitch attitude can be excluded as a potential source of any extra power required.

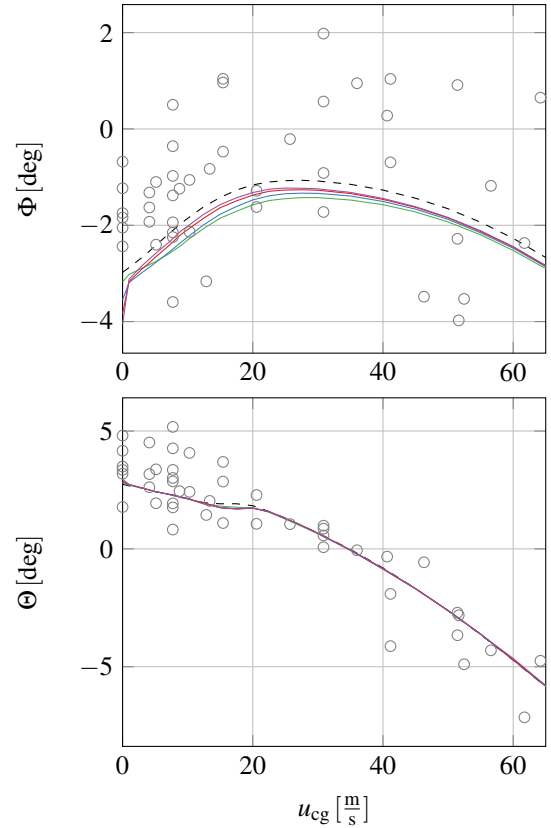


Fig. 4: Roll angle, Φ , and pitch angle, Θ , over forward flight velocity, u_{cg} . Results obtained by the fully-coupled dynamic inflow model for $N_{lbm} = 32$ (—), 64 (—), 128 (—), and 192 (—). Pitt-Peters model (---) and flight test measurements (○) for comparison.

The roll attitude, Φ , did not contribute to the parasitic power of the fuselage because the drag polar was not dependent on Φ . It is worth noting that neither the choice of the inflow model nor the resolution of the fully-coupled model notably changed the predicted pitch attitude. As the position of the center of gravity was kept constant, this implies that the pitching moment of the rotor was of the same magnitude for both the fully-coupled and the Pitt-Peters inflow models. The predicted roll attitude showed qualitative agreement with the measurements, but due to the high scattering of the flight test data further comparisons were difficult.

Comparing the control inputs necessary for trimmed forward flight (shown in Fig. 5), the predicted collective inputs correlated well up to about $u_{cg} = 40 \frac{m}{s}$, with the fully-coupled model performing better than the Pitt-Peters model, except for the hover case. In hover, the fully-coupled dynamic inflow model did not show convergence with increasing resolution of the fluid solver. At forward speeds greater than $u_{cg} = 40 \frac{m}{s}$ the collective input was underpredicted by both models, which correlated well with the corrected main rotor power shown in Fig. 3. To compare collective inputs from the flight tests with the models, the measured data had to be corrected by 26.35%. This was done because of the specific collective calibration used in

the flight tests, which zeroed the collective input when the blade pitch angle at $0.75R$ was zero.

The pedal input (shown in the second plot of Fig. 5) showed high scatter in the recorded flight test data. Nevertheless, qualitative agreement of the fully-coupled model and the Pitt-Peters model with the measurements was found. Similar to the collective, the pedal input showed increasing differences to the measured data at speeds greater than $u_{cg} = 30 \frac{m}{s}$.

The lateral input of the fully-coupled model showed a strong dependency on the resolution of the fluid solver, as shown in the third plot of Fig. 5. Although convergence for the hover state was not found, in forward flight the lateral input converged for the resolutions $N_{lbm} = 128$ and higher. For these resolutions, the fully-coupled model showed the same trends as the flight test data and the Pitt-Peters model. The constant offset from the flight test data suggested to come from calibration in the testing, although this was not clear. Nevertheless, it is shown that the fully-coupled inflow model correctly predicted the trends, including the reversal in the low-flight-speed regime, which was previously shown to be an important factor for model performance [18].

Regarding the longitudinal cyclic input, also shown in Fig. 5, both predictive models gave similar results, which were independent of the resolution of the fluid solver. Similar to the lateral input, the reason for the constant offset between the models and the flight test data was not clear. Nevertheless, both models correctly predicted the trends for the cyclic inputs required for trimmed stationary forward flight.

The necessity of lateral input in slow forward flight is caused by the non-uniformity of the inflow between the forward and the aft blades [18]. This variation is expressed by the cosine component of the induced velocity, v_c^i , which is shown in Fig. 6 along with the other components of the induced inflow velocity as defined by Pitt and Peters [1]. For the cosine component, a clear dependence on the resolution N_{lbm} of the fluid solver was observed, which caused a comparable convergence behavior as for the lateral cyclic input shown previously; see Fig. 5.

Chen's investigation [19] of various inflow models in slow forward flight showed that the peak of v_c^i was located at a velocity value smaller than two times the mean induced velocity, v_0^i , in hover. This was also true for the Pitt-Peters inflow model as well as for the fully-coupled inflow model as used in the current study; see Fig. 6. Furthermore, Chen found [19] that the cosine coefficient of the inflow calculated by the Pitt-Peters model correlated well with measurements. The cosine component of the inflow velocity predicted by the fully-coupled inflow model correlated well with the results from the Pitt-Peters model, although a strong dependence on the resolution of the fluid flow computations was also observed.

The sine component, v_s^i , as predicted by the fully-coupled model did not agree with the Pitt-Peters model,

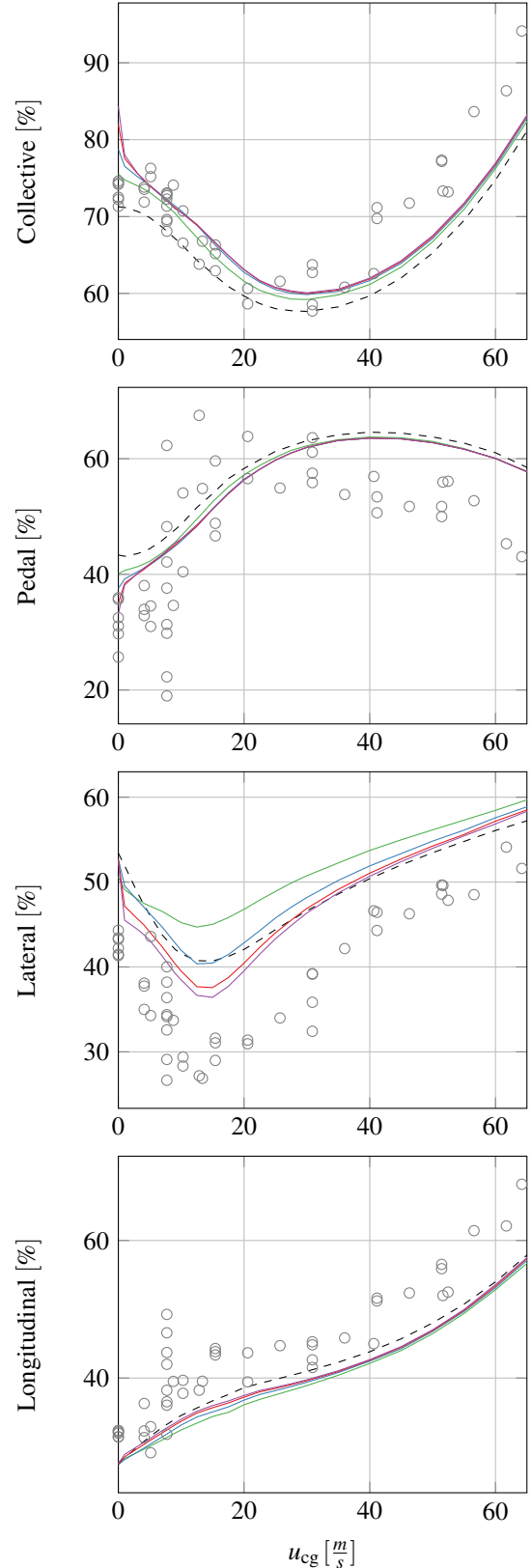


Fig. 5: Collective, pedal, lateral, and longitudinal cyclic input in trimmed forward flight obtained by the fully-coupled model for $N_{lbm} = 32$ (—), 64 (—), 128 (—), and 192 (—). Pitt-Peters model (---) and flight test measurements (\circ) for comparison.

which could be caused by the fuselage that was modeled with wall boundary conditions in the fluid solver, therefore influencing the flow. Nevertheless, as the magnitudes of the sine components were very small compared to the cosine components, their influence on the helicopter motion was also comparatively small. The mean inflow component predicted by the fully-coupled model correlated well with the Pitt-Peters model except for hover, which came from the discussed convergence problems in this case and needs to be investigated further.

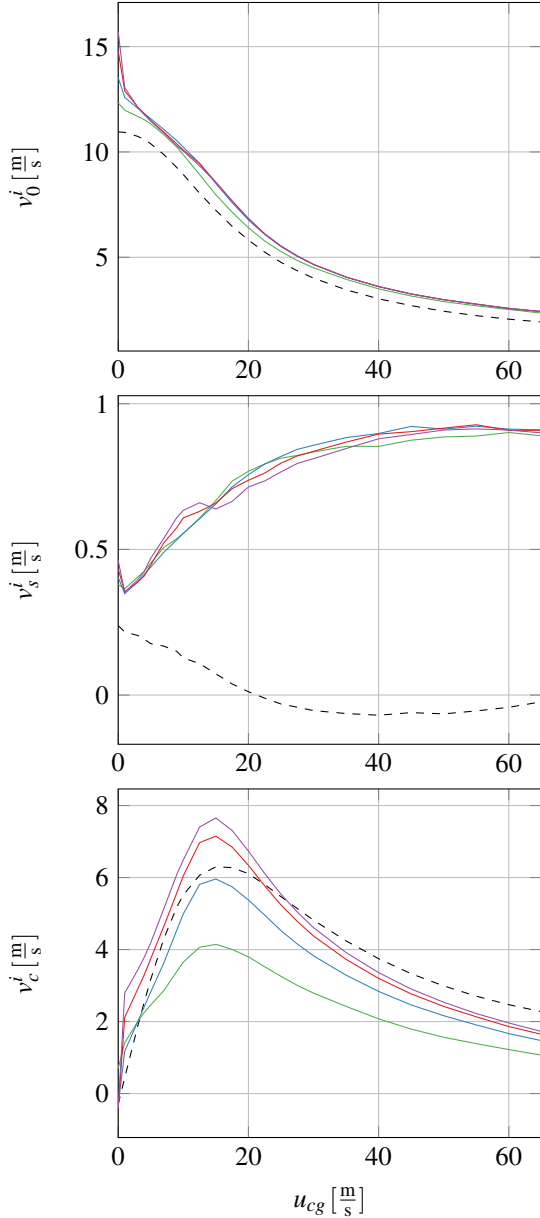


Fig. 6: Mean v_0^i , sine v_s^i , and cosine v_c^i components as used by Pitt and Peters [1]. Values of the fully-coupled model for $N_{lbm} = 32$ (—), 64 (—), 128 (—), and 192 (—). Corresponding values from the Pitt-Peters model (---) for comparison.

Dynamic Reaction to Pilot Inputs

The predicted results in trimmed stationary forward flight of the fully-coupled model for $N_{lbm} \geq 128$ and the Pitt-Peters model correlated well with the flight test data for flight speeds up to $u_{cg} = 40 \frac{m}{s}$. Therefore, the following investigation of the dynamic reaction to pilot inputs focused on the flight speed regime below $u_{cg} = 40 \frac{m}{s}$ and excluded hover. To investigate the dynamic behavior of the helicopter model, the reactions to doublet inputs in the lateral, longitudinal, and collective in slow forward flight were compared to the corresponding flight test results; see Figs. 7–9. As the trim for these flight conditions differed between the models and the flight tests, the inputs necessary for the trimmed flight were subtracted from the time history of the inputs, resulting in differential inputs to the trimmed state that are indicated by a preceding Δ .

Remember that when using the steady-state rotor assumption in transient maneuvers, the rotor reacts instantaneously to changes in the inflow or the controls. Nevertheless, for low-frequency control inputs or low-frequency variations of the inflow, in previous work this assumption was found valid because the blade motion adjusted after about one rotor revolution, which is very fast compared to the reaction of the rotorcraft [15]. To evaluate the influence of the steady-state rotor assumption on the resulting helicopter motion, results using the Pitt-Peters model with and without steady-state assumption were also included.

Aside from the influence on the flight dynamics, the steady-state assumption had an influence on the main rotor power. Because of the enforced main rotor relative rotational speed of 100%, the power showed high-frequency oscillations that were not present in the results without the steady-state rotor assumption; see Figs. 7–9. This outcome originated from the suppression of a continuous flapping variation over time by the steady-state rotor assumption, because it enforced a steady flapping reaction of the rotor in each timestep of the calculation. This high-frequency oscillation did not influence the response of the computed helicopter motion, because it was filtered by the inertia of the fuselage.

Excluding the last row, the following figures are ordered so as to show the response of the helicopter grouped by axes. The roll axis pilot input and system response are shown in the first (i.e., left) column, the pitch axis input and response in the second column, and the yaw axis input and response in the third (i.e., right) column. Aside from the pilot cyclic, pedal, and collective inputs (shown in the first row from top), vehicle angular velocities (second row from top), and the attitudes (third row from top) are shown. The descent rate (calculated from the vertical speed indicator), the main rotor relative rotational speed, N/N_0 , and the main rotor power are shown in the last row; see Figs. 7–9.

The first maneuver that was analyzed was a doublet input to the right in the lateral cyclic at a forward flight speed of $u_{cg} = 13.37 \frac{m}{s}$; see Fig. 7. The collective, which is not

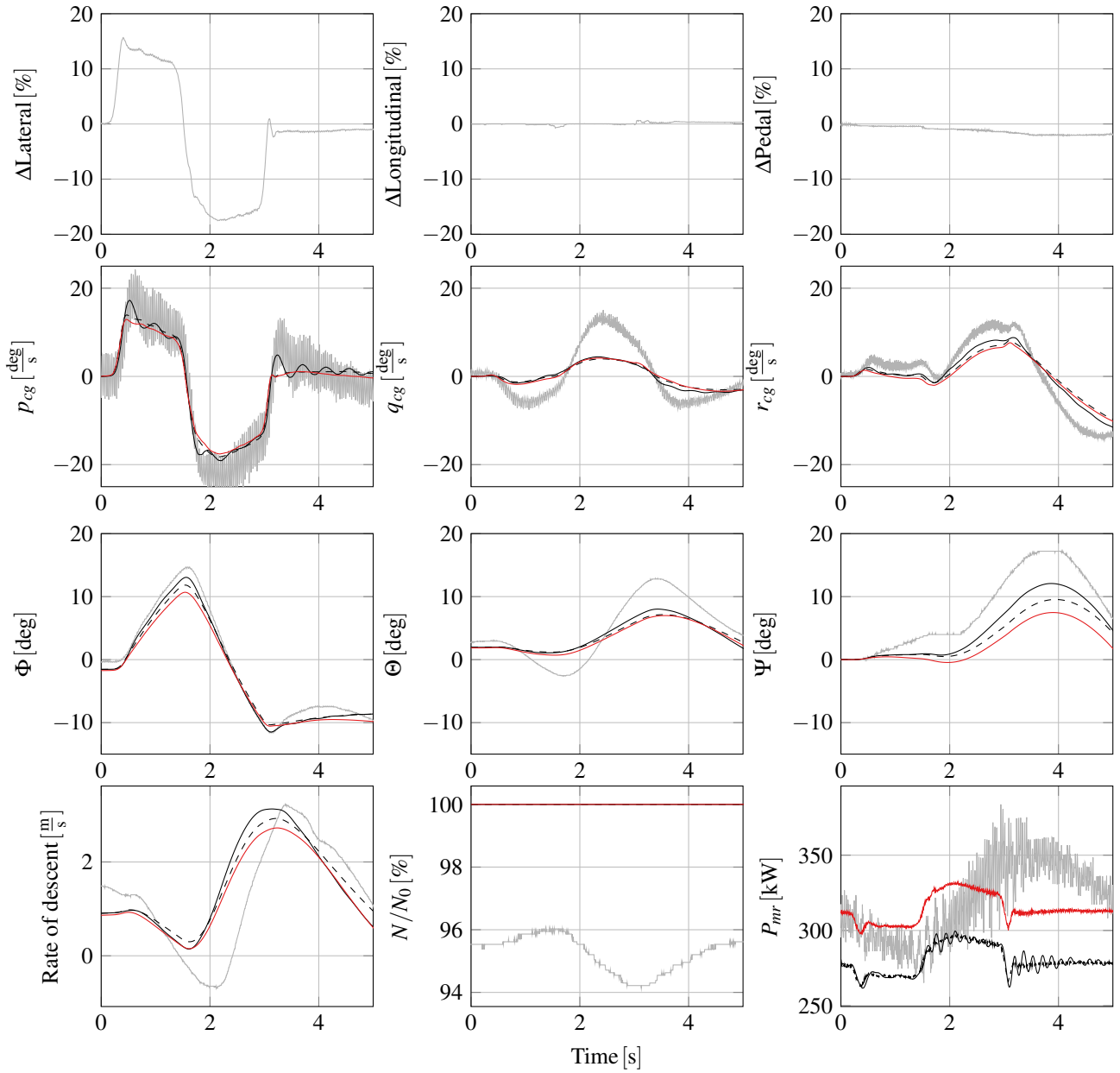


Fig. 7: Reaction of the helicopter to a doublet right in the lateral cyclic at $u_{cg} = 13.37 \frac{\text{m}}{\text{s}}$ using the fully-coupled dynamic inflow model with $N_{lbm} = 128$ (—) and the Pitt-Peters model with (---) and without steady-state rotor assumption (—). Flight test measurements (—) for comparison. Pilot inputs at constant collective in the first row, angular velocities in the cg -system, p_{cg} , q_{cg} , r_{cg} , in the second row, and attitudes, Φ , Θ , Ψ , in the third row. Rate of descent and rotor relative rotational speed, N/N_0 , together with the required main rotor power, P_{mr} , in the last row.

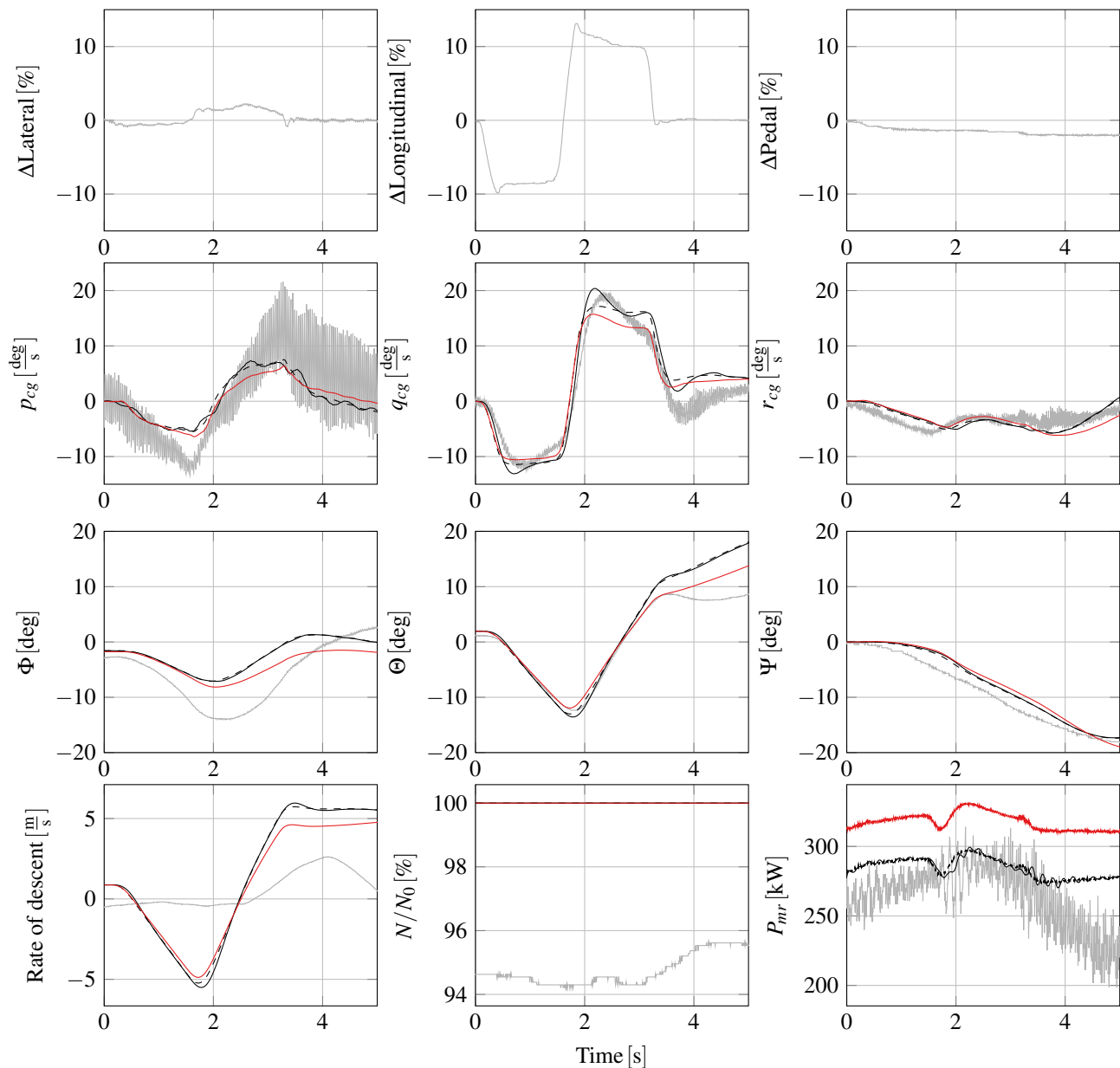


Fig. 8: Reaction of the helicopter to a doublet push in the longitudinal cyclic at $u_{cg} = 12.86 \frac{\text{m}}{\text{s}}$ using the fully-coupled dynamic inflow model with $N_{lbm} = 128$ (—) and the Pitt-Peters model with (---) and without steady-state rotor assumption (—). Flight test measurements (—) for comparison. Pilot inputs at constant collective in the first row, angular velocities in the cg -system, p_{cg}, q_{cg}, r_{cg} , in the second row, and attitudes, Φ, Θ, Ψ , in the third row. Rate of descent and rotor relative rotational speed, N/N_0 , together with the required main rotor power, P_{mr} , in the last row.

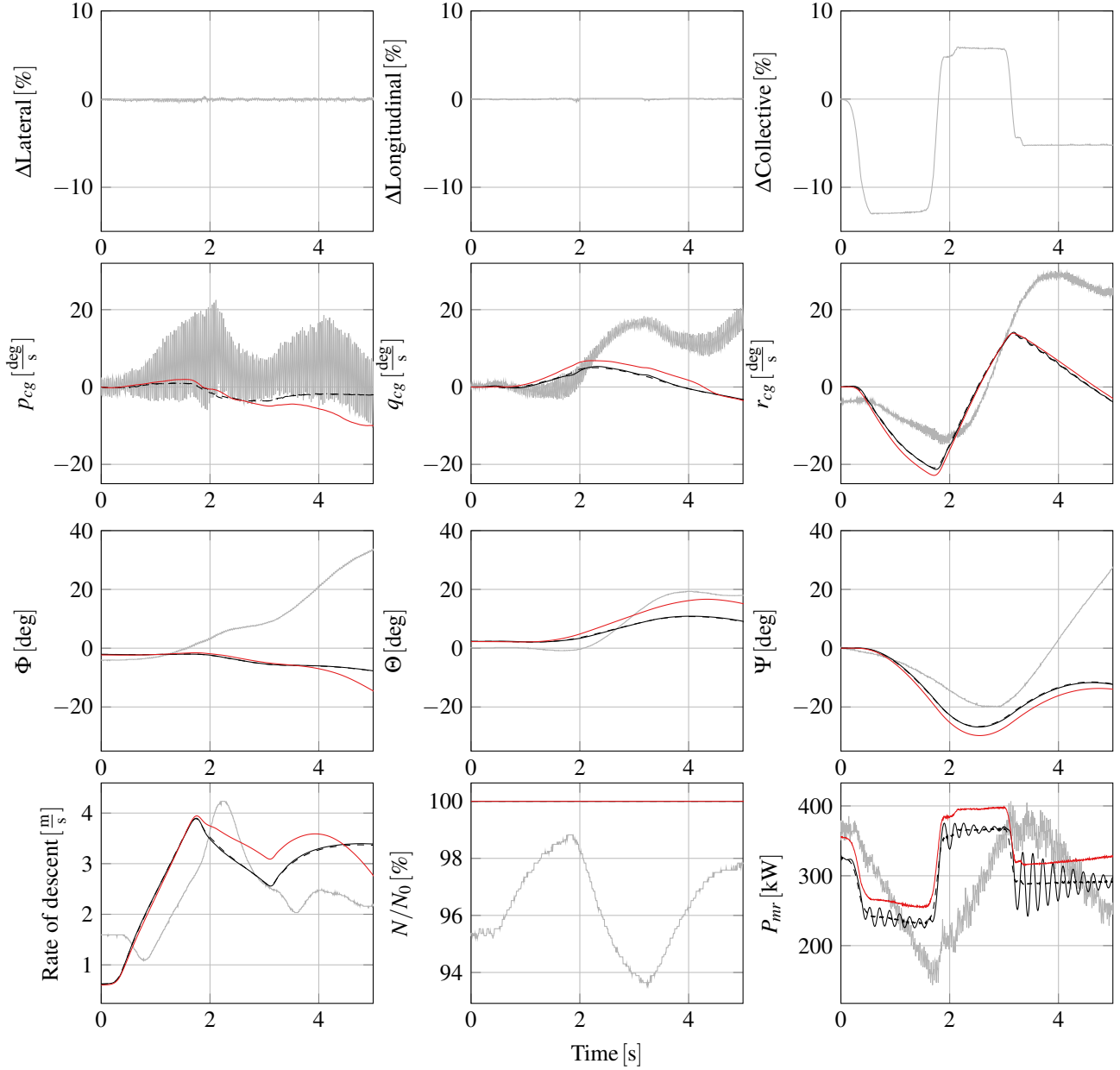


Fig. 9: Reaction of the helicopter to a doublet push in the collective at $u_{cg} = 7.72 \frac{\text{m}}{\text{s}}$ using the fully-coupled dynamic inflow model with $N_{lbm} = 128$ (—) and the Pitt-Peters model with (---) and without steady-state rotor assumption (—). Flight test measurements (—) for comparison. Pilot inputs at constant pedal in the first row, angular velocities in the cg -system, p_{cg}, q_{cg}, r_{cg} , in the second row, attitudes, Φ, Θ, Ψ , in the third row. Rate of descent and rotor relative rotational speed, N/N_0 , together with the required main rotor power, P_{mr} , in the last row.

shown, was held constant for the test period. The resulting on-axis response described by the rolling angular velocity, p_{cg} , was predicted well by both the fully-coupled model and also the Pitt-Peters model. Nevertheless, the Pitt-Peters model without the steady-state assumption for the rotor correlated better with the flight test data, which can also be seen in the better agreement in the roll attitude, Φ . The low-frequency oscillations in p_{cg} indicated that the blade flapping motion was excited extensively and did not reach the steady state within one rotor revolution. Unfortunately, the flight test data of p_{cg} were subjected to significant high-frequency oscillations, which prevented a more detailed analysis of the low-frequency behavior of p_{cg} .

Regarding the off-axis response shown in the pitching angular velocity, q_{cg} , neither the fully-coupled nor the Pitt-Peters model showed the correct amplitude that was observed in the flight test. Nevertheless, all models showed the correct trends and phasing in the time domain. The same held for the pitch attitude, Θ . The angular velocity in yawing direction, r_{cg} , showed good agreement with the flight test data for the fully-coupled and the Pitt-Peters inflow models, although its magnitude was slightly underpredicted. The rate of descent was not trimmed to zero in the flight test. Its trends were predicted correctly, whereas the amplitudes were slightly underpredicted, which was true for both inflow models. As the power required for the main rotor changed during the maneuver, the main rotor relative rotational speed, N/N_0 , also changed due to the absence of an automatic engine control in the Bo-105. These effects were not modeled, which prevented a meaningful comparison between model and flight test. Nevertheless, these quantities were included for completeness.

The doublet push in the longitudinal cyclic input at constant collective, that was selected as second maneuver for the comparison, was conducted at a forward speed of $u_{cg} = 12.86 \frac{m}{s}$; see Fig. 8. As in the previous maneuver, the on-axis response (shown here by the pitching angular velocity, q_{cg}) agreed well with the flight test for the fully-coupled and the Pitt-Peters models. This also manifested in an excellent agreement of the pitch attitude, Θ , with the flight test data. The steady-state rotor assumption had a significant influence on q_{cg} , which becomes evident when comparing the results without this assumption to the flight test data, because then the reaction of the helicopter to the overshoots in the longitudinal input were captured. Both models reacted faster to the input than the helicopter in the flight test, as can be seen in the instance of the first push in the longitudinal cyclic and the system response in the angular velocity q_{cg} .

Concerning the off-axis response in p_{cg} , both the fully-coupled model and the Pitt-Peters inflow model showed an underprediction of the helicopter's response. Nevertheless, trend and phasing were predicted correctly. Consequently, the same held for the roll angle, Φ . Given the relatively low magnitude of the angular velocity in yawing direction, r_{cg} , the predictions correlated well with the flight test for both models and did not show an influence of the steady-state as-

sumption. The same held for the resulting yawing attitude, Ψ . For the descent rate, the predicted results and the flight test did not correlate. Neglecting the noise in the power measurements and given the significant pilot input in the longitudinal cyclic, the power required and the relative rotational speed of the main rotor, N/N_0 , did not show much variation during the flight test when compared to other maneuvers (e.g., the collective input shown in Fig. 9).

A doublet push in the collective with constant lateral, longitudinal, and pedal at a forward flight speed of $u_{cg} = 7.72 \frac{m}{s}$ is shown in Fig. 9. Without an engine control system, the relative rotational speed of the rotor, N/N_0 , varied significantly during the flight test, whereas in the computations, N/N_0 was fixed at 100%. The increase and following decrease of the rotor speed (that resulted from the sudden change in collective input) yielded corresponding varying power requirements in the flight test. However, as a result from the fixed rotor rotational speed in the modeling, the changes in the required power were caused solely by the changes in collective, yielding a curve that resembled the collective input time history.

The rate of descent of the flight test was not predicted well, independently of the used dynamic inflow model. Nevertheless, the same trends are seen if the phase offset of the computations is neglected. For the rolling angular velocity, p_{cg} , and the resulting roll attitude, Φ , the computations differed significantly from the flight test measurements. The same held for the pitching angular rate, q_{cg} . Despite this outcome, the resulting pitch attitude, Θ , computed by the fully-coupled model showed similar magnitudes as the flight test. The angular velocity in yawing direction, r_{cg} , was not trimmed to zero at the start of the doublet push (in the flight tests), which was also reflected in the yaw attitude, Ψ . Apart from that, yaw predictions showed the correct trends, with an offset in the magnitudes for both the fully-coupled and the Pitt-Peters model. Except for the oscillations in the main rotor power, the steady-state assumption did not change the vehicle dynamic reaction predicted by the Pitt-Peters model for the investigated maneuver, which indicated the validity of the steady-state rotor assumption for this case.

Summary and Conclusions

A fully-coupled, real-time-capable fluid dynamics/flight dynamics simulation was developed, that was validated against flight test data measured with a MBB Bo-105 helicopter. The comparison of pilot control inputs, attitudes, and power required in trimmed stationary forward flight showed the capability of the new inflow modeling approach in the fully-coupled fluid dynamics/flight dynamics simulation to correctly predict the vehicle behavior. The convergence study in the lateral input indicated that this only holds for resolutions of $N_{lbn} = 128$ or higher. This behavior originated from the need to correctly calculate the forward-aft variation of the inflow velocity, which was heavily resolution dependent. Although giving good results for for-

ward flight speeds up to $u_{cg} = 40 \frac{\text{m}}{\text{s}}$, no convergence in the required power and control inputs was found for the hover case, which needs to be investigated further. For the converged computations, the new model's predictions were as accurate as the results from the Pitt-Peters model.

To evaluate the dynamic system response to pilot inputs, three maneuvers with increasing complexity in aeromechanic couplings were compared to flight test data and to results obtained using the Pitt-Peters inflow model. For the maneuvers that imposed a perturbation of the cyclic, good agreement was found in the on-axis response. Without the steady-state rotor assumption, the Pitt-Peters model correlated better with the flight test data, which highlighted the introduced restrictions due to this assumption. Therefore, modeling without the steady-state rotor assumption is desired.

The off-axis response was found to agree in shape but underestimated the amplitudes for the maneuvers that used cyclic inputs. The underprediction was similar to the results obtained using the Pitt-Peters inflow model instead of the new modeling approach. This behavior was also observed by Lewis [18], and shown by Rosen [20] to be caused by wake distortions. The maneuver with a doublet push in the collective indicated the need to correctly model the engine and the inertia of the rotor system (to capture the variations in the rotational speed) to improve the correlation of the computational model and the flight test data, independently of the used inflow model.

Aside from proving the potential of the new fully-coupled inflow model, the investigation highlighted deficiencies in the helicopter model and the inflow model which need to be addressed. To correctly predict the required power of the main rotor at high forward flight speeds, the correct drag polar for the fuselage (including velocity dependencies) will be necessary. Following the discussion on the conducted convergence study, the resolution of the Lattice-Boltzmann fluid dynamics solver that is still computable in real-time has to be increased. While shown results were obtained using one single graphics card, this brings up the need to further parallelize the computations not only on multiple GPUs but also on multiple graphics cards (or a GPU cluster).

After incorporating these improvements and proving the validity, this real-time-capable, physics-based, fully-coupled model can be used for piloted flight simulations. In the next steps, the prediction of the rotorcraft flight dynamics and handling qualities in time-varying ground effect and in the airwake of ships and other objects has to be validated for the model to reach its full potential. Without the need for prior knowledge of the flow field or flight conditions, the model will provide the capability to better train pilots for complicated flight situations such as ship deck landings, or flight in the complicated wake of large objects such as skyscrapers, urban environment or mountainous regions, reducing the risk of serious flight incidents.

Acknowledgments

The authors would like to thank the DLR for providing the flight test data and especially Dr. von Grünhagen for his support and the discussions during data evaluation. We would also like to thank the U.S. Office of Naval Research for supporting this work under grant award N62909-16-1-2118. The technical monitors were Dr. Isaac Bankman and Dr. Kenneth Iwanski.

REFERENCES

- [1] Pitt, D. M., and Peters, D. A., "Rotor Dynamic Inflow Derivatives and Time Constants From Various Inflow Models," Ninth European Rotorcraft Forum, 1983.
- [2] Peters, D. A., Boyd, D. D., and He, C. J., "A Finite-State Induced-Flow Model for Rotors in Hover and Forward Flight," *Journal of the American Helicopter Society*, Vol. 34 (4), October 1989.
- [3] Zhao, J., Prasad, J. V. R., and Peters, D. A., "Rotor Wake Distortion Model for Helicopter Maneuvering Flight," *Journal of the American Helicopter Society*, Vol. 49 (4), October 2004.
- [4] Gennaretti, M., Gori, R., Cardito, F., Serafini, J., and Bernadini, G., "A Space-Time Accurate Finite-State Inflow Model for Aeroelastic Applications," 72nd Annual Forum of the American Helicopter Society, West Palm Beach, FL, 2016.
- [5] Peters, D. A., "How Dynamic Inflow Survives in the Competitive World of Rotorcraft Aerodynamics – The Alexander Nikolsky Honorary Lecture," *Journal of the American Helicopter Society*, Vol. 54, 2009.
- [6] Polsky, S., Wilkinson, C. H., Nichols, J., Ayers, D., Mercado-Perez, J., and Davis, T. S., "Development and Application of the SAFEDI Tool for Virtual Dynamic Interface Ship Airwake Analysis," AIAA SciTech, San Diego, CA, 2016.
- [7] Owen, I., and Padfield, G. D., "Integrating CFD and piloted simulation to quantify ship-helicopter operating limits," *Aeronautical Journal*, 2006.
- [8] Amsellem, D., Cortial, J., and Farhat, C., "Towards Real-Time CFD-Based Aeroelastic Computations Using a Database of Reduced-Order Information," *AIAA Journal*, Vol. 48, 2010.
- [9] Rubenstein, G., Moy, D. M., Sridharan, A., and Chopra, I., "A Python-based Framework for Real-time Simulation using Comprehensive Analysis," 72nd Annual Forum of the American Helicopter Society, West Palm Beach, FL, 2016.

- [10] Bludau, J., Rauleder, J., Friedmann, L., and Hajeck, M., "Real-time Simulation of Dynamic Inflow Using Rotorcraft Flight Dynamics Coupled With a Lattice-Boltzmann Based Fluid Simulation," 55th Aerospace Sciences Meeting, AIAA SciTech, Grapevine, TX, 2017.
- [11] Peters, D. A., and Haquang, N., "Dynamic Inflow for Practical Applications," *Journal of the American Helicopter Society*, Vol. 33 (4), 1988.
- [12] Meldi, M., Vergnault, E., and Sagaut, P., "An Arbitrary Lagrangian-Eulerian Approach for the Simulation of Immersed Moving Solids with Lattice Boltzmann Method," *Journal of Computational Physics*, Vol. 235, 2013.
- [13] Leishman, J. G., *Principles of Helicopter Aerodynamics*, 2nd edition, Cambridge University Press, 2006.
- [14] Mei, R., Luo, L. S., and Shyy, W., "An Accurate Curved Boundary Treatment in the Lattice Boltzmann Method," ICASE Report No. 2000-6, 2000.
- [15] Johnson, W., *Helicopter Theory*, 2nd edition, Dover Publications, 1994.
- [16] Cooke, A. K., and Fitzpatrick, E. W. H., *Helicopter Test and Evaluation*, 1st edition, QinetiQ Limited, 2002.
- [17] Johnson, W., *Rotorcraft Aeromechanics*, 1st edition, Cambridge University Press, 2013.
- [18] Lewis, W. D., "An Aeroelastic Model Structure Investigation for a Manned Real-Time Rotorcraft Simulation," 49th Annual Forum of the American Helicopter Society, St. Louis, MO, 1993.
- [19] Chen, R. T. N., "A Survey of Nonuniform Inflow Models for Rotorcraft Flight Dynamics and Control Applications," 15th European Rotorcraft Forum, 1989.
- [20] Rosen, A., and Isser, A., "A New Model of Rotor Dynamics during Pitch and Roll of a Hovering Helicopter," *Journal of the American Helicopter Society*, Vol. 40 (5), 1995.